Distinct mechanisms of CB1 and $GABA_B$ receptor presynaptic modulation of striatal indirect pathway projections to mouse Globus Pallidus

Giacomo Sitzia[1,2], Karina Possa Abrahao[3], Daniel Liput[1], Gian Marco Calandra[4], David M. Lovinger*[1]

[1] Current address: Laboratory for Integrative Neuroscience, National Institute on Alcohol Abuse and Alcoholism, US National Institutes of Health, Rockville, USA

[2] Molecular Neurophysiology Laboratory, Department of Physiology and Pharmacology, Karolinska Institutet, Stockholm, Sweden

[3] Departamento de Psicobiologia, Universidade Federal de São Paulo, Campus São Paulo, São Paulo, SP, Brazil

[4]Institute for Stroke and Dementia Research, Ludwig-Maximilians-Universität, Munich, Germany.

Email: Giacomo.sitzia@ki.se, lovindav@mail.nih.gov

Corresponding Author information:

*David M. Lovinger (lovindav@mail.nih.gov).

Laboratory for Integrative Neuroscience, National Institute on Alcohol Abuse and Alcoholism, National Institutes of Health, Maryland, 20852, USA

Orcid: 0000-0002-5454-6725

Key Points

P/Q-type are the predominant VGCC controlling presynaptic Ca^{2+} and GABA release on the striatal indirect pathway projections

$GABA_B$ receptor modulate of iSPN-GPe projections via a VGCC- dependent mechanism

CB1 receptors modulate iSPN-GPe projections via a VGCC- independent mechanism

Abstract

Presynaptic modulation is a fundamental process regulating synaptic transmission. Striatal indirect pathway projections originate from A2A- expressing spiny projection neurons (iSPNs), targeting the globus pallidus external segment (GPe) and control the firing of the tonically active GPe neurons via GABA release. It is unclear if and how the presynaptic GPCRs, $GABA_B$ and CB1 receptors, modulate iSPN-GPe projections. Here we used an optogenetic platform to study presynaptic Ca^{2+} and GABAergic transmission at iSPN projections, using a genetic strategy to express the calcium sensor GCaMP6f or the excitatory channelrhodopsin (hChR2) on iSPNs. We found that P/Q-type calcium channels are the primary VGCC-subtype controlling presynaptic calcium and GABA release at iSPN-GPe projections. N-type and L-type VGCCs contribute to GABA release at iSPN-GPe synapses. $GABA_B$ receptor activation resulted in a reversible inhibition of presynaptic Ca^{2+} transients (PreCaTs) and an inhibition of GABAergic transmission at iSPN-GPe synapses. CB1 receptor activation did not inhibit PreCaTs while inhibiting GABAergic transmission at iSPN-GPe projections. CB1 effects on GABAergic transmission persisted in experiments where Na_V and K_V1 were blocked, indicating a VGCC- and K_V1 independent presynaptic mechanism of action of CB1 receptors. Taken together, presynaptic modulation of iSPN-GPe projections by CB1 and $GABA_B$ receptors is mediated by distinct mechanisms.

Introduction

The dorsal striatum (DS) is the main input structure of the basal ganglia (BG), a group of subcortical regions involved in motor control, associative learning and decision making. Spiny projection neurons (SPNs) constitute up to 95% of neurons in the rodent striatum (Graveland & Di Figlia, 1985). SPNs are classified based on their molecular markers and projection targets into direct pathway SPNs (dSPNs) and indirect pathway SPNs (iSPNs) (Gerfen et al., 1990). The dSPNs express the dopamine D1 receptor and project to the substantia nigra pars reticulata (SNr), the entopeduncular nucleus (EPN) and, through axonal collaterals, to the globus pallidus external segment (GPe) (Chang et al., 1981). iSPNs express dopamine D2 and adenosine A2A receptors and project to the GPe. Neurons in the GPe are tonically active, and this activity is influenced by GABAergic inputs from the iSPNs. Presynaptic neuromodulation by GPCRs including $GABA_B$ and CB1 controls GABA release in the GPe (Engler et al., 2006; Kaneda & Kita, 2005) but the synapse- specific effects and mechanisms of action are

56 unclear. Thus, understanding how GPCRs govern presynaptic calcium entry and neurotransmitter release
57 at the iSPN projections to the GPe will allow to better determine how the striatum controls its downstream targets,
58 in physiology and in disease.
59 Two key modulators of GABAergic transmission in the GPe are the $G_{i/o}$ coupled cannabinoid type 1 (CB1) and
60 $GABA_B$ receptors. Expression levels of CB1 receptors on striatal terminals in the GPe and SNr are among the
61 highest in the CNS (Davis et al., 2018; Hu & Mackie K., 2015). The expression levels of CB1 receptors in the GPe
62 have been shown to drop dramatically when striatopallidal projections are lesioned (Hernkenham et al., 1991) or if
63 CB1 receptors are genetically knocked out from SPNs (Bonm et al., 2021). To date, it remains unclear whether
64 pallidal neurons express functional CB1 receptors. CB1 receptors control GABA release in the GPe (Engler et al.,
65 2006) but it is unknown what set of GABAergic synapses mediates this effect. Sources of extra-striatal GABAergic
66 inputs in the GPe include local collaterals (Ketzef et al., 2021; Higgs et al., 2021) and GPi inputs (Weglage et al.,
67 2022). $GABA_B$ receptors are expressed on striatopallidal projections (Chen et al, 2004). $GABA_B$ receptors exert pre-
68 synaptic effects by reducing GABA release at GABAergic synapses in the GPe but also act postsynaptically to
69 inhibit GPe neurons (Kaneda & Kita, 2005). Overall, it remains unclear if and how CB1 and
70 $GABA_B$ receptors modulate transmission specifically at iSPN-GPe projections.
71 CB1 and $GABA_B$ receptors suppress neurotransmitter release in the CNS through signaling cascades mediated by
72 the $G_{\beta\gamma}$ subunit, including inhibition of voltage-gated calcium channels (VGCCs), inhibition of the vesicle release
73 complex downstream of VGCCs and activation of K^+channels (Araque et al., 2017; Chalifoux & Carter, 2011).
74 Mechanisms involving the $G_{\alpha i}/G_o$ subunits, including the inhibition of cAMP/ PKA signaling, also influence
75 neurotransmitter release (Araque et al., 2017; Chalifoux & Carter, 2011). The downstream mechanisms engaged by
76 CB1 and $GABA_B$ receptors are synapse specific and can be non- canonic. In the nucleus accumbens (NAc), CB1
77 receptors suppress neurotransmitter release at cortico-accumbal synapses through a VGCC-independent, K^+
78 channel-dependent mechanism (Robbe et al., 2001), while $GABA_B$ receptors inhibit neurotransmitter release at
79 glutamatergic synapses through a VGCC-independent, SNAP25-dependent mechanism (Manz et al., 2019). In the
80 DS, $GABA_B$ receptors suppress neurotransmitter release at corticostriatal synapses via a VGCC-dependent
81 mechanism (Kupfershmidt & Lovinger, 2015).
82 Here we studied the presynaptic mechanisms of action of CB1 and $GABA_B$ receptors on the iSPN-GPe projections.
83 We validated a slice photometry approach to measure presynaptic Ca^{2+} at iSPN-GPe projections, using transgenic
84 mice expressing the Ca^{2+} indicator GCaMP6f in iSPNs (A2aCre-GCaMP6f mice). We also used transgenic mice
85 expressing the excitatory opsin channelrhodopsin (hChR2) to study the mechanisms regulating CB1 and $GABA_B$
86 receptors effects on GABAergic transmission at iSPN-GPe synapses. We found that P/Q-type VGCCs are the
87 primary VGCCs mediating Presynaptic Calcium Transients (PreCaTs) and GABAergic transmission at iSPN
88 synapses in the GPe. N- and L-type VGCCS inhibition reduced GABAergic transmission, although with a smaller
89 effect size than P/Q-type VGCCs, but not PreCaTs. $GABA_B$ receptor activation decreased PreCaTs and GABAergic

transmission. Conversely, CB1 receptor activation at iSPN projections did not decrease PreCaTs, while reducing GABAergic transmission. CB1 effects persisted when potassium voltage-gated channels 1 (K_V1) and sodium voltage gated channels (Na_V) were blocked, and reduced the frequency of miniature inhibitory postsynaptic currents (mIPSCs), which we found to be insensitive to the VGCC blocker cadmium in the GPe. Taken together, our results indicate that CB1 receptor inhibition of GABA release at iSPN terminals is mediated by a K_V1, Na_V and VGCC-independent mechanism.

Methods

Ethical approval

Experiments were conducted in accordance with the National Institutes of Health's Guidelines for Animal Care and Use, and all experimental procedures were approved by the National Institute on Alcohol Abuse and Alcoholism Animal Care and Use Committee (Protocol LIN-DL-1).

Animals

Mice were housed in groups of 2-4 in the NIAAA vivarium on a 12 hr light cycle with ad libitum access to food and water. B6;129S-Gt(ROSA)26Sortm95.1(CAG-GCaMP6f)Hze/J (GCaMP6f) and B6.Cg-Gt(ROSA)26Sortm32(CAG-COP4*H134R/EGFP)Hze/J (Ai14-ChR2) mice were purchased from The Jackson Laboratory (JAX; Bar Harbor, ME, USA). B6.FVB(Cg)-Tg(Adora2a-cre)KG139Gsat/Mmucd (A2A-Cre) mice were purchased from the Mutant mouse resource and research centers (MMRRC, 030869, Davis, CA, USA). These mutant mouse lines were maintained by breeding with wildtype C57BL6J mice purchased from JAX. Experimental animals were generated by breeding male or female mice homozygous for the GCaMP6f or ChR2 allele with mice heterozygous for the A2A-Cre alleles to restrict GCaMP6f or ChR2H134R (hChR2) expression to striatal indirect pathway SPNs. Male and female mice (aged 3-24 weeks) were included in the electrophysiology and slice photometry experiments experiments. No differences were observed in effect sizes of the drugs used across different ages. Male mice were used to validate GFP expression in GCaMP6f mice (aged 70w). Genotyping was performed by polymerase chain reaction (PCR) on genomic DNA from ear biopsies.

Immunohistochemistry and confocal imaging

A2aGCaMP6 f mice (n = 3), were anesthetized with pentobarbital (50 mg/ kg) prior to the transcardiac perfusion of 1x PBS, followed by 4% formaldehyde (FA) (4% paraformaldehyde in 1x PBS). Brains were kept in 4% FA overnight and then transferred to 1x PBS until slicing. Free-floating sections (50 mM) were cut using a Pelco easySlicer Vibratome (Ted Pella Inc., Redding, Ca, USA). Slices were washed 3 x 5 minutes in 1x PBS, and then incubated in a blocking solution containing 5% normal goat serum in PBS-T (0.2% Triton X-100). Slices were then incubated for 48 hr at 4C in 1x PBS containing the primary antibodies (Chicken anti-GFP, AbCam cat. No. #13970. 1:2000; Rabbit anti-NeuN, Cell Signaling Technology, cat. No. #24307, 1:1000). Slices were then washed 3 x 5

124 minutes in 1x PBS and incubated in 1x PBS containing the secondary antibodies for 2 hours (Alexa Fluor 488,
125 Goat-anti-chicken, Invitrogen A11039, 1:500; Alexa Fluor 594 goat anti-rabbit, Invitrogen A11012, 1:500). A final
126 wash of 3 x 5 minutes was performed prior to mounting using DAPI Fluoromount-G® (Southern Biotech, Cat No.
127 0100-20). Slices were imaged on a Zeiss LSM 800 laser confocal scan head mounted on a Zeiss Z1Axio Observer
128 inverted microsope frame (Carl Zeiss, Oberkochen, Germany). An argon laser was used for 488 excitation (Alexa
129 Fluor 488, dichroic MBS 488/594, emission 497-590), a HeNe594 laser for 594 excitation (Alexa Fluor 594,
130 dichroic MBS 488/561, emission 598-670). Objectives used for imaging included a C-Apochromat 63x/1.2 NA W
131 Korr M27 (Zeiss) and Plan-Apochromat 20x/0.8 NA.
132
133 **Brain slice preparation for slice photometry and patch-clamp experiments**
134 Mice were anesthetized with isoflurane and decapitated after assessing deep anesthesia by tail-pinch. The brain was
135 rapidly collected and transferred to a slicing chamber filled with ice-cold sucrose-based cutting solution containing
136 the following (in mM): 194 sucrose, 30 NaCl, 4.5 KCl, 26 $NaHCO_3$, 1.2 NaH_2PO_4, 10 D -glucose, 1 $MgCl_2$,
137 saturated with 95% O_2/5% CO_2. Coronal sections (250-300 μm) containing the GPe were obtained using a Leica
138 VT1200S Vibratome (Leica Microsystems, Buffalo Grove, IL) and rapidly moved to an incubation chamber filled
139 with artificial cerebrospinal fluid (aCSF) containing (in mM): 124 NaCl, 4.5 KCl, 26 $NaHCO_3$, 1.2 NaH_2PO_4, 10
140 D-glucose, 1 $MgCl_2$, and 2 $CaCl_2$, saturated with 95% O_2/5% CO_2. Slices were incubated for 30-60 minutes at 32°C
141 and then maintained at room temperature prior to recording. The same slicing protocol was used for slice photometry
142 and patch-clamp experiments.
143
144 **Slice photometry**
145 Photometry recordings were acquired using a Zeiss upright epifluorescence microscope equipped with a 40x/0.8
146 NA water immersion objective. Slices were placed in a recording chamber and superfused at ~2 mL min-1 with
147 aCSF maintained at ~30°C. GCaMP6f was excited using either a mercury HBO lamp, gated with a uniblitz shutter
148 (Vincent Associates, Rochester, NY, USA) or a 470 nm LED (ThorLabs, Newton, NJ, USA) and filtered at 470 ±
149 20 nm. Excitation power was measured at the sample plane using a microscope slide photodiode power sensor
150 (ThorLabs) and was 3.8 mW for the mercury HBO lamp and <1.0 mW for the 470 nm LED. Emitted light was
151 collected and filtered at 525 ± 25 nm, passed through a 180 μm2 diaphragm and directed to a photomultiplier tube
152 (PMT; Model D-104, Photon Technology International, Edison, NJ, USA). The PMT output was filtered at 1 kHz
153 and digitized at 6.67 kHz using a Digidata 1322A and Clampex pClamp 10.6 software (Axon Instruments,
154 Molecular Devices LLC, Sunnyvale, CA, USA). A bipolar stimulating electrode was placed in the lateral GPe, just
155 inside the border between the striatum and GPe, and the 180 μm^2 field of view was positioned just lateral to the
156 electrode tip. Photometry sweeps were acquired every 30 seconds. During each sweep, after an initial rapid decay
157 in fluorescence, a presynaptic calcium transient was evoked by a train of 4 electrical pulses at 10Hz. Slices were

158 equilibrated to the recording chamber conditions and electrical stimulation for ~20 min to allow for response
159 stabilization. Photometry sweeps were averaged over 2 minutes (4 sweeps) before calculating peak ΔF/F values for
160 electrically evoked presynaptic calcium transients (PreCaTs). For experiments using the mercury HBO lamp, the
161 baseline fluorescence intensity tended to decay throughout the entire sweep so a baseline correction procedure was
162 employed as described previously (Kupferschmidt and Lovinger, 2015). However, for experiments using the LED,
163 the baseline fluorescence intensity tended to stabilize prior to evoking presynaptic calcium transients so the baseline
164 correction procedure was omitted.
165
166 **Whole-cell patch-clamp recordings**
167 Hemislices were transferred to a recording chamber perfused with aCSF at 30–32 °C with a ~2 ml/min flow rate.
168 Neurons were visualized with an upright microscope (Scientifica, Uckfield, East Sussex, UK) using a LUMPlanFL
169 N × 40/0.80 NA W objective (Olympus, Waltham, MA). Recordings from GPe neurons were obtained using
170 micropipettes (2–4 MΩ) made from 1.5 mm OD/1.12 mm ID borosilicate glass with a filament (World Precision
171 Instruments, Sarasota, FL) pulled with a P-97 puller (Sutter Instruments Novato, CA).
172 Recordings were performed using a Multiclamp 700A amplifier and a Digidata 1322A or Multiclamp 700B and a
173 digidata 1550B digitizer using a low-pass filter of 2 kHz and a sampling frequency of 10 kHz. Data were analyzed
174 using pClamp 10.3 or pClamp 10.6 software (Molecular Devices, Sunnyvale, CA). Most experiments were
175 performed filling micropipettes with a high-chloride solution containing (in mM): 150 CsCl, 10 HEPES, 2.0 $MgCl_2$,
176 0.3 Na-GTP, 3.0 Mg-ATP, 0.2 BAPTA-4Cs, 5 QX-314. Validation of neurotransmitter release at iSPN-GPe
177 projections (Fig. 1) was performed filling micropipettes with a low-chloride solution containing (in mM): 114
178 CsMeSO3, 5.0 NaCl, 1.0 TEA-Cl, 10 HEPES, 5.0 QX-314, 1.1 EGTA, 0.3 Na-GTP, 4.0 Mg-ATP. Recordings were
179 obtained in voltage clamp mode and neurons were clamped at -45 mV unless specified differently (Fig. 1). $GABA_A$
180 mediated spontaneous (sIPSCs) and optically evoked (oIPSCs) were isolated through the bath-perfusion of aCSF
181 containing the AMPA receptor blocker DNQX (10 μM) and NMDA receptor blocker DL-AP5 (50 μM) and
182 abolished by Gabazine application (Fig. 1). To monitor series resistance (range <30 MΩ) throughout the recording,
183 a 10mV, 50-100 ms depolarizing step was applied every minute; cells were excluded if series resistance varied
184 >20% during the recording.
185 Optogenetic stimulation protocols: Blue light (470 nm) was delivered through a 4-channel LED driver (ThorLabs,
186 MD, USA). In most experiments oIPSCs were evoked using a train of 4 pulses delivered at 10 Hz. Prior to the start
187 of the recording the light intensity (range 0.4- 6 mW) or the pulse width (0.4-2 ms) were adjusted to obtain a stable
188 oIPSC. For the electrophysiological experiments presented in Fig. 1 and the experiment in fig. 4 where oIPSCs
189 were recorded in presence of TTX+ 4-AP, a 5 ms stimulus with a stimulation intensity of ~10 mW was used to
190 ensure maximal stimulation of presynaptic terminals. As indicated in Fig. 1, oIPSCs were TTX-sensitive and
191 Gabazine sensitive.

192

193 **Drugs**

194 Stocks of ω-conotoxin GVIA, ω-agatoxin IVA, (R)-Baclofen, DNQX disodium salt, TTX, 4-AP and DL-AP5
195 sodium salt were dissolved in ddH2O. WIN55,212-2 mesylate and nifedipine were dissolved in 100% DMSO. All
196 drug stocks were stored at -20°C and diluted in aCSF just prior to superfusion. QX-314 bromide was dissolved fresh
197 in internal solution. ω-conotoxin GVIA and ω -agatoxin IVA were purchased form Alomone Labs (Jerusalem,
198 Israel), QX-314 bromide and 4-AP from Millipore Sigma (St. Louis, MO, USA), and all other drugs from Tocris
199 Biosciences (Minneapolis, MN, USA).

200

201 **Statistical Analysis**

202 Statistical analysis was performed in GraphPad Prism (GraphPad Software, La Jolla, California) and Excel.
203 Significance was set at $p < 0.05$ in all analyses. All data are reported as mean + SD. Exact P values for all
204 comparisons are reported in the main text and all figure legends. Statistical significance is indicated in the figures
205 and figure legends. For all photometry and electrophysiology experiments, except for sIPSC and mIPSC
206 experiments, the data are expressed as % of baseline (defined as the average of the last 8 - 10 minutes recorded
207 prior to drug application). One-way rmANOVA or mixed-effect analysis with no correction followed by Tukey's
208 multiple comparisons test was performed in experiments where 3 time points were compared (baseline: average of
209 minute 3-8 of baseline; drug: last 2 minutes of drug application, washout: last 2 minutes of washout). Two-way
210 rmANOVA with no correction followed by Tukey's multiple comparisons test was performed to compare the effects
211 of application of different VGCC blockers on PreCaTs and oIPSCs. Experiments where 2 time points (baseline,
212 drug) were compared were analyzed using paired t-test, if the difference between pairs followed a normal
213 distribution assessed through the Shapiro-Wilk test, or Wilcoxon matched pairs test when not normally distributed.

214

215 **Results**

216 **An optogenetic strategy to study presynaptic calcium transients and GABAergic transmission at indirect**
217 **pathway projections to the GPe**

218 To study presynaptic calcium and GABAergic transmission at iSPN-GPe projections we crossed Adora2a -Cre
219 (A2a-Cre) mice with either GCaMP6f mice or AiCOP4 mice to express GCaMP6f or hChR2 in iSPNs. We imaged
220 EYFP fluorescence in A2a-AiCOP4 mice and found high expression in the dorsal striatum, GPe, but not in the SNr
221 (Fig. 1A). Using immunohistochemistry, we quantified the percentage of striatal neurons expressing GCaMP6f in
222 the A2aCre-GCaMP6f mice. We labeled neurons using the pan-neuronal marker NeuN and GFP to visualize
223 GCaMP6f- expressing cells and found that on average 42.9 + 4.9 % of striatal neurons expressed GFP (n = 3 mice,
224 5 micrographs/ mouse; n cells expressing GFP/ n of cells expressing NeuN in each mouse: 461/1021, 396/1064,
225 486/1050), indicating GCaMP expression in ~ half of the striatal SPNs (Fig. 1B) in accordance with previous reports

226 (Graveland & Di Figlia, 1985). No GCaMP6f- expressing cell somata was found in the GPe, and sparse labeling
227 was observed in the cortex. We functionally assessed the A2a-AiCOP4 line by performing whole-cell patch clamp
228 recordings in the GPe (fig. 1C). We first assessed neurotransmission at iSPN-GPe synapses. We used a low-chloride
229 intracellular and first recorded optically evoked postsynaptic currents while clamping the membrane potential near
230 the sodium reversal potential (~0mV). The outward current recorded at this holding potential was decreased by
231 Gabazine to 7 + 4.8 % of baseline (Fig. 1C) (n = 6 cells from n = 3 mice, paired t-test $p < 0.0001$). Next, we clamped
232 the neurons near the chloride reversal potential (~ -45 mV) and recorded no current at this potential in 5/ 6 neurons.
233 In 1/6 neurons, a DNQX and DL-AP5 insensitive, TTX sensitive current emerged. Taken together, these results
234 indicate that optical stimulation of iSPN-GPe projections in the A2aCre-AiCOP4 line evokes GABA release. Next,
235 we assessed whether the recorded oIPSCs were TTX- sensitive and monosynaptic (Fig. 1D). We found that TTX
236 application abolished oIPSCs (amplitude decreased to 1 + 1.4 % of baseline), and oIPSC amplitude was restored to
237 195 + 60.9% of baseline by TTX + 4-AP co-application (n = 5 cells from n = 4 mice; mixed-effect analysis, $F_{(2, 11)}$
238 , treatment effect $p < 0.0001$; Tukey's multiple comparisons test: baseline vs TTX $p = 0.0021$; Baseline vs TTX +
239 4- AP = 0.0023; TTX vs TTX + 4-AP $p < 0.0001$) (Fig. 1E). These results indicate that the oIPSCs were TTX-
240 sensitive and monosynaptic, also according to their onset latency (Fig. 1F) (low-chloride, cells from 1D: 3.6 + 1.4
241 ms; high-chloride, cells from 1E: 1.2 + 0.37 ms) (Cho et al., 2013; Petreanu et al., 2009). We next tested whether
242 the PreCaTs evoked in the GPe through local electrical stimulation (Fig. 1G) were activity- dependent and Ca^{2+}
243 dependent. In the first experiment, we delivered stimuli of increasing intensity using 100 µA increments (range 0
244 µA- 700 µA) and found that the PreCaTs amplitude increased with stimulation intensity, indicating its activity-
245 dependency (Fig. 1H) (n = 5 slices from n = 4 mice; one-way rmANOVA, $F_{(7,28)} = 26.7$, $p < 0.0001$). In the second
246 experiment, we followed the PreCaTs amplitude during a baseline period of 10 minutes, and next we switched the
247 recording solution from normal ACSF to Ca^{2+}-free ACSF. The PreCaT amplitude decreased to 29.1 + 7 % of
248 baseline during Ca^{2+}- free ACSF application, and re-application of normal ACSF partially restored the PreCaTs to
249 50.8 + 12.5 % of baseline (Fig. 1I, J) (n = 5 slices, n = 4 mice one-way rmANOVA, Treatment: $F_{(2,8)} = 71.94$; $p <$
250 0.0001; Tukey's multiple comparisons test: Ca^{2+} free vs baseline $p < 0.0001$; washout vs baseline $p < 0.0001$;
251 washout vs Ca^{2+} free $p = 0.0186$). In summary, these validation steps indicated that the A2aCre-GCaMP6f and
252 A2aCre-AiCOP4 lines represent a bona fide approach to study presynaptic calcium and GABA release from iSPN
253 to GPe neurons.
254

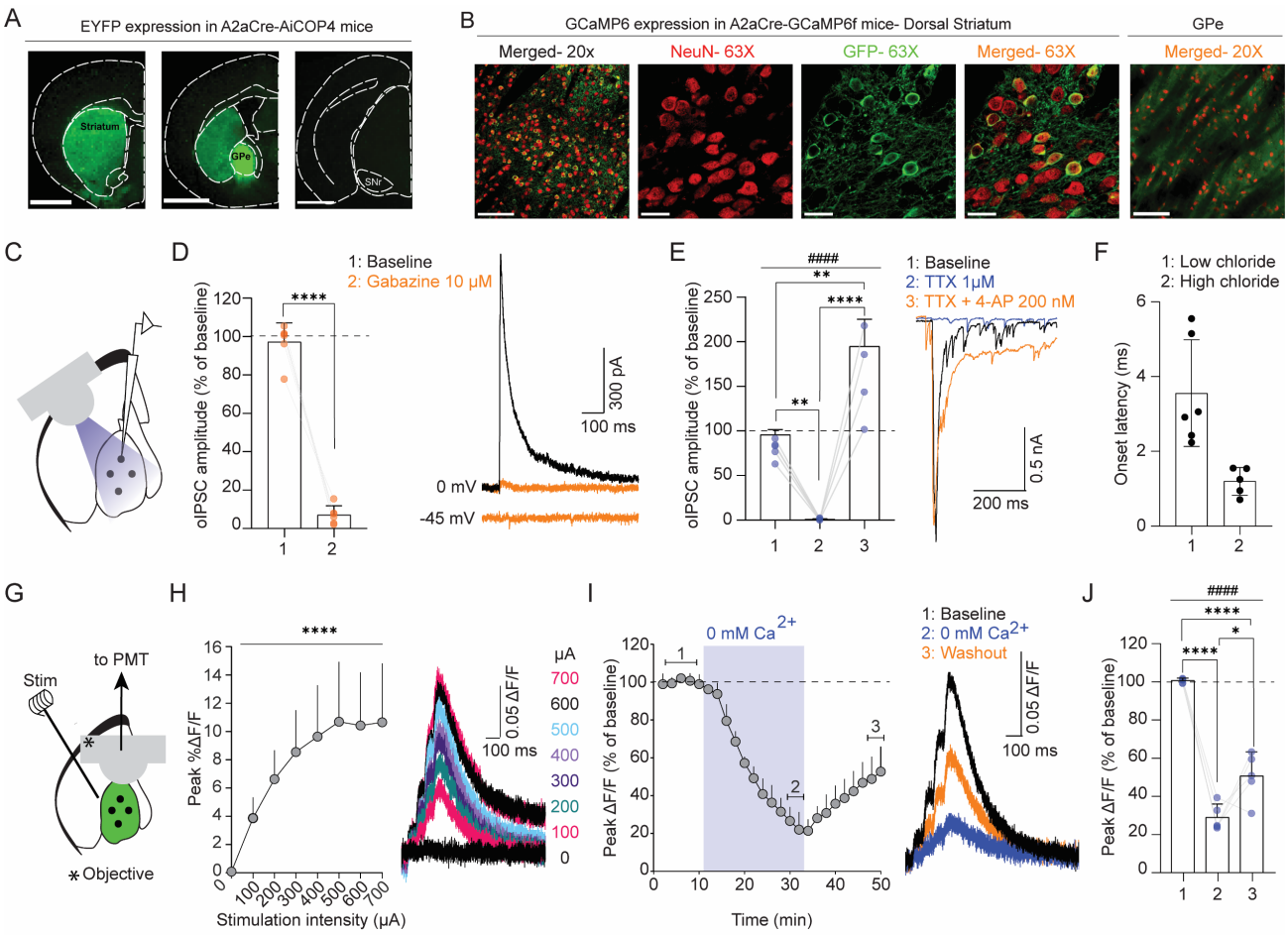

Figure 1. An optogenetic strategy to study GABAergic transmission and PreCaTs at iSPN-GPe projections **A**: Representative micrographs of EYFP expression in the A2aCre-AiCOP4 line. From left to right: coronal slices containing the dorsal striatum, GPe and SNr. Dense EYFP fluorescence was observed in the striatum and GPe, not in the SNr. **B**: Representative confocal micrographs where IHC staining was performed in A2aCre-GCaMP6f mice using anti-GFP (green) and anti-NeuN (red). From left to right: 20x images of dorsal striatum (scale bar: 100 μM); 63x images of NeuN, GFP and the two channels merged in the dorsal striatum (scale bar: 25μM); 20x image of GPe (scale bar: 100 μM). **C:** Diagram of optogenetic and whole-cell patch clamp experiments. **D**: Summary bar graph and example traces of oIPSC inhibition by Gabazine. Gabazine fully inhibited oIPSCs recorded at iSPN-GPe synapses indicating their $GABA_A$ dependency (n = 6 cells from n = 3 mice). **E**: Summary bar graph and example traces of whole-cell patch clamp experiments where (1) baseline, (2) TTX effect and (3) TTX + 4-AP effects were compared. TTX fully inhibited oIPSCs, which were restored above baseline levels by TTX+ 4-AP application (n = 5 cells from n = 4 mice). **F**: onset latency of oIPSCs recorded using high chloride or low chloride intracellular solutions, cells from panels D and E. **G**: schematic of slice photometry experiments. **H**: Input/output (I/O) curve experiment. The amplitude of the PreCaTs scaled with stimulation intensity indicating activity- dependence (n = 5 slices, n = 4 mice). **I:** Time course of Ca^{2+} free ACSF application effects on PreCaTs. **G:** Bar graph summary of effects: baseline, last 2 minutes of Ca^{2+} free ACSF, last 2 minutes of washout (n = 5 slices from n = 4 mice). * $P < 0.05$; ** $P < 0.001$; *** $P < 0.0001$ ****/ #### $P < 0.0001$.

P/Q-type are the predominant VGCC controlling presynaptic Ca^{2+} and GABAergic transmission at the indirect pathway projections to the GPe

We performed a series of experiments to characterize the VGCCs mediating PreCaTs and GABAergic transmission at iSPN-GPe projections. We studied the effects of the bath application of selective blockers of P/Q type, N-type or L-type VGCCs on PreCaTs (Fig. 2A, B). Application of the P/Q-type VGCC blocker, ω-agatoxin IVA (ATX, 200 nM), decreased PreCaTs amplitude to 71.7 + 12.7 % of baseline and 53.3 + 18.5 % of baseline after washout (n = 6 slices from n = 6 mice, one-way rmANOVA, Treatment: $F_{(2, 10)} = 32.53$; $p < 0.0001$; Tukey's multiple comparisons test: Baseline vs ATX p = 0.0017; Baseline VS Washout p < 0.0001; ATX VS Washout p = 0.0266). Application of the N-type VGCC blocker, ω-Conotoxin GVIA (CTX, 1 μM), did not significantly decrease in PreCaTs amplitude, which was 85.2 + 11.3 % of baseline after drug and 78 + 17.3 % of baseline following washout (n = 8 slices from n = 8 mice, one-way rmANOVA, Treatment: $F_{(2, 14)} = 8.38$; p = 0.004; Tukey's multiple comparisons test: Baseline vs CTX p = 0.0565; Baseline VS Washout p = 0.0032; CTX VS Washout p = 0.322). Bath application of the L-type VGCC blocker, Nifedipine (10 μM), did not decrease PreCaTs amplitude at iSPN-GPe projections, which was 95 + 5.6 % of baseline and 90.2 + 7.8 % after washout (n= 5 slices from n = 5 mice, one-way rmANOVA, Treatment: $F_{(2, 8)} = 3.638$, P = 0.0752). Two-way rmANOVA comparison of ATX, CTX and Nifedipine application effects on PreCaTs at iSPN-GPe projections revealed a significant interaction between the time (timepoints analyzed: baseline, drug, washout) and drug factors, indicating a difference in the effect of the 3 blockers on PreCaTs (Time X drug: $F_{(4, 32)} = 6.933$; p = 0.0004; agatoxin vs nifedipine p = 0.004). Overall, these results indicate that P/Q type VGCCs are the primary controllers of PreCaTs at iSPN-GPe terminals. Next, we examined the effects of the bath application of selective blockers of P/Q type, N-type or L-type VGCCs on GABAergic transmission (Fig. 2C, D). Application of ATX induced a decrease in oIPSC amplitude to 20.2 + 14.4 % of baseline which persisted at 8.6 + 7.2 % of baseline after washout (iSPN-GPe, one-way rmANOVA, n = 5 cells from n = 4 mice, Treatment: $F_{(2, 8)} = 189.1$; $p < 0.0001$; Tukey's multiple comparisons test: Baseline vs ATX p < 0.0001; Baseline vs Washout p < 0.0001; ATX VS Washout p = 0.1172). Application of CTX induced a significant decrease in oIPSC amplitude to 73.2 + 12.7% of baseline which persisted at 69 + 22.6 % of baseline after washout (n = 5 cells from n = 4 mice, one-way rmANOVA, Treatment: $F_{(2, 8)} = 8.4$; p = 0.0108; Tukey's multiple comparisons test: Baseline VS CTX p = 0.0275; Baseline VS Washout: p = 0.0133; CTX VS Washout p =0.8689). Application of Nifedipine induced a significant decrease in oIPSC amplitude to 78.9 + 11.1 % of baseline which persisted at 80.6 + 12.9 % of baseline after washout (n= 5 cells from n = 4 mice, one-way rmANOVA, Treatment: $F_{(2, 8)} = 10.97$, P = 0.0051; Tukey's multiple comparisons test: Baseline VS Nifedipine p = 0.0074; Baseline VS Washout p = 0.0115; Nifedipine VS Washout p = 0.9437). Two-way RM ANOVA comparison of ATX, CTX and Nifedipine application effects on oIPSCs at iSPN-GPe synapses revealed a significant interaction between the time (timepoints analyzed: baseline, drug washout) and drug factors (Time X drug: $F_{(4, 24)} = 21.09$; p < 0.0001; Tukey's multiple comparisons test: agatoxin vs conotoxin p < 0.0001; agatoxin vs nifedipine p < 0.0001).

Taken together, these results indicate that P/Q type VGCCs are the primary VGCC involved in GABAergic transmission at iSPN-GPe synapses. In contrast, N-type and L-type VGCCs play a significant but smaller role.

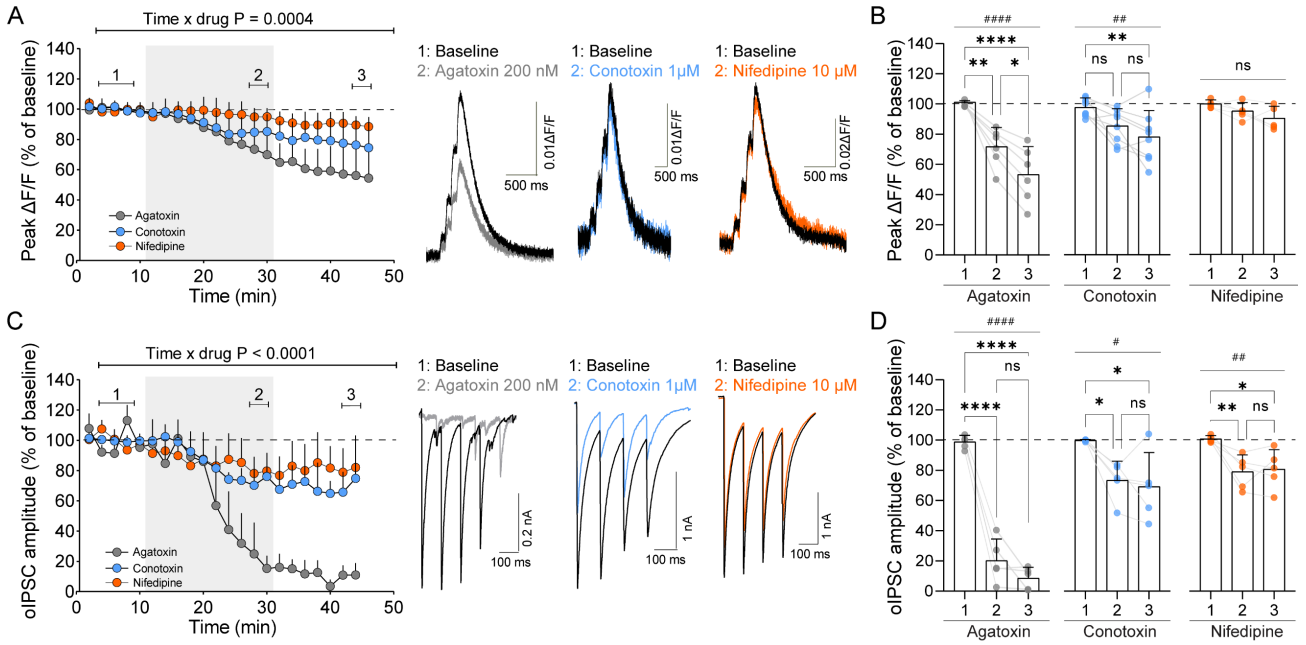

Figure 2: P/Q-type are the predominant VGCC controlling presynaptic Ca^{2+} and GABAergic transmission at the indirect pathway projections to the GPe. A: Timecourse of VGCC blocker application effects on PreCaTs and raw photometry traces. B: Summary of drug effects: baseline, last 2 minutes of drug, last 2 minutes of washout. Blockade of P/Q -type VGGCs (Agatoxin, n = 6 slices from n = 6 mice) significantly decreased PreCaTs from baseline, whereas no significant effect on PreCaTs was observed by blocking N-type VGCCs (Conotoxin, n= 8 slices from n = 8 mice) or L-type VGCCs (Nifedipine, n = 5 slices from n = 5 mice). C: Timecourse of VGCC blocker application effects on oIPSCs and raw electrophysiological traces. D: Comparison of drug effects: baseline, last 2 minutes of drug, last 2 minutes of washout. Blockade of P/Q -type VGGCs (Agatoxin, n = 5 cells from n = 4 mice) significantly decreased PreCaTs from baseline, and smaller but significant effects were induced by blocking N-type VGCCs (Conotoxin, n = 5 cells from n = 4 mice) or L-type VGCCs (Nifedipine, n = 5 cells from n = 4 mice). * $p < 0.05$; **/ ## $P < 0.01$; *** $P < 0.0001$; ****/ #### $P < 0.0001$.

VGCC-dependent modulation of iSPN-GPe projections by $GABA_B$ receptors

We studied the effects of $GABA_B$ receptor activation on PreCaTs at iSPN-GPe projections (Fig. 3A, B). Bath application of the $GABA_B$ agonist Baclofen (10 μM) decreased PreCaTs amplitude to 45.7 + 15.1 % of baseline which persisted at 50.8 + 23.3 % of baseline after washout (n = 7 slices from n = 5 mice, one-way rmANOVA, Treatment: $F_{(2, 12)} = 40.94$; $p < 0.0001$; Tukey's multiple comparisons test: Baseline VS Baclofen $p < 0.0001$; Baseline VS Washout $p < 0.0001$; Washout VS Baclofen $p = 0.7323$). To test whether Baclofen application induced a long-term depression of PreCaTs at iSPN-GPe projections we performed a second experiment of pulse-chase where Baclofen application was followed by the application of the $GABA_B$ antagonist CGP 35358 (2 μM) (Fig. 3C, D). Bath application of Baclofen decreased PreCaTs amplitude to 46.5 + 12.7 % of baseline, an effect that was

reversed by CGP 35358 which brought PreCaTs to 107.5 + 23 % of baseline (n = 5 slices from n = 2 mice, one-way rmANOVA, Treatment: $F_{(2, 8)} = 23.10$; p = 0.0005; Baseline vs Baclofen p = 0.0014; Baseline VS CGP p = 0.7848; Baclofen VS CGP p = 0.0007).

We next examined the effects of $GABA_B$ receptor activation on oIPSCs at iSPN-GPe projections (Fig. 3E, F). Bath application of the $GABA_B$ agonist Baclofen decreased the oIPSC amplitude to 49.8 + 16 % of baseline (n = 7 cells from n = 5 mice, paired t-test, p = 0.0002). To determine the site of action of $GABA_B$ receptors in the GPe we analyzed sIPSCs (Fig. 3G). We found that Baclofen application induced a significant decrease in sIPSC frequency from baseline 4 + 2.1 Hz to Baclofen 2.3 + 2.7 Hz and amplitude from baseline 55.7 + 25.4 pA to Baclofen 47 + 22 pA (n = 12 cells from n = 10 mice; Frequency: paired t-test, p = 0.0195; Amplitude: paired t-test, p < 0.0001). The observed sIPSC decrease induced by baclofen application is indicative of a presynaptic effect, whereas a change in amplitude might reflect an effect on multivesicular release or a shift in the population of synapses contributing to the sIPSCs. Taken together, these experiments indicate that $GABA_B$ receptor modulation of iSPN-GPe projections is reversible VGCC- mediated and involves presynaptic modulation of GABA release.

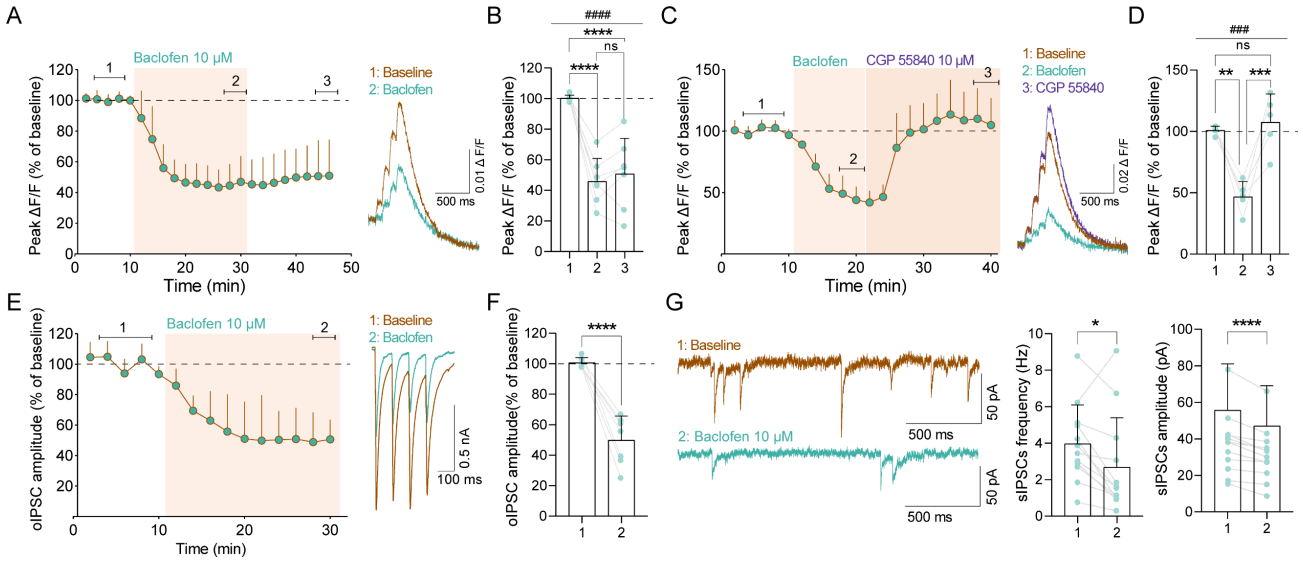

Figure 3: VGCC-dependent modulation of iSPN-GPe projections by GABAB receptors. A: Time course of Baclofen effects on PreCaTs and raw photometry traces. **B:** Summary of drug effects: baseline, last 2 minutes of drug, last 2 minutes of washout. $GABA_B$ activation (Baclofen, n = 7 slices from n = 5 mice) significantly decreased PreCaTs amplitude. **C:** Time course experiment of Baclofen followed by CBP 55840 effects on PreCaTs **D:** Baclofen significantly decreased PreCaTs and CGP55840 application reversed PreCaTs to baseline levels (n = 5 slices from n = 2 mice). **E:** Time course of Baclofen effects on oIPSCs at iSPN-GPe synapses and raw electrophysiological traces. **F:** Baclofen significantly reduced oIPSCs at iSPN-GPe terminals (n = 7 cells from n = 5 mice). **G:** Effects of Baclofen application on sIPSCs. Example traces and summary bar graphs. Baclofen application significantly decreased the frequency and amplitude of sIPSCs recorded in the GPe, indicating a pre-synaptic site of action (n= 12 cells from n = 10 mice). * p < 0.05; **/ ## P < 0.001; ***/ ### P < 0.001; ####/ **** P < 0.0001.

VGCC- and K_V1- independent mechanisms of presynaptic modulation of iSPN-GPe projections by CB1 receptors

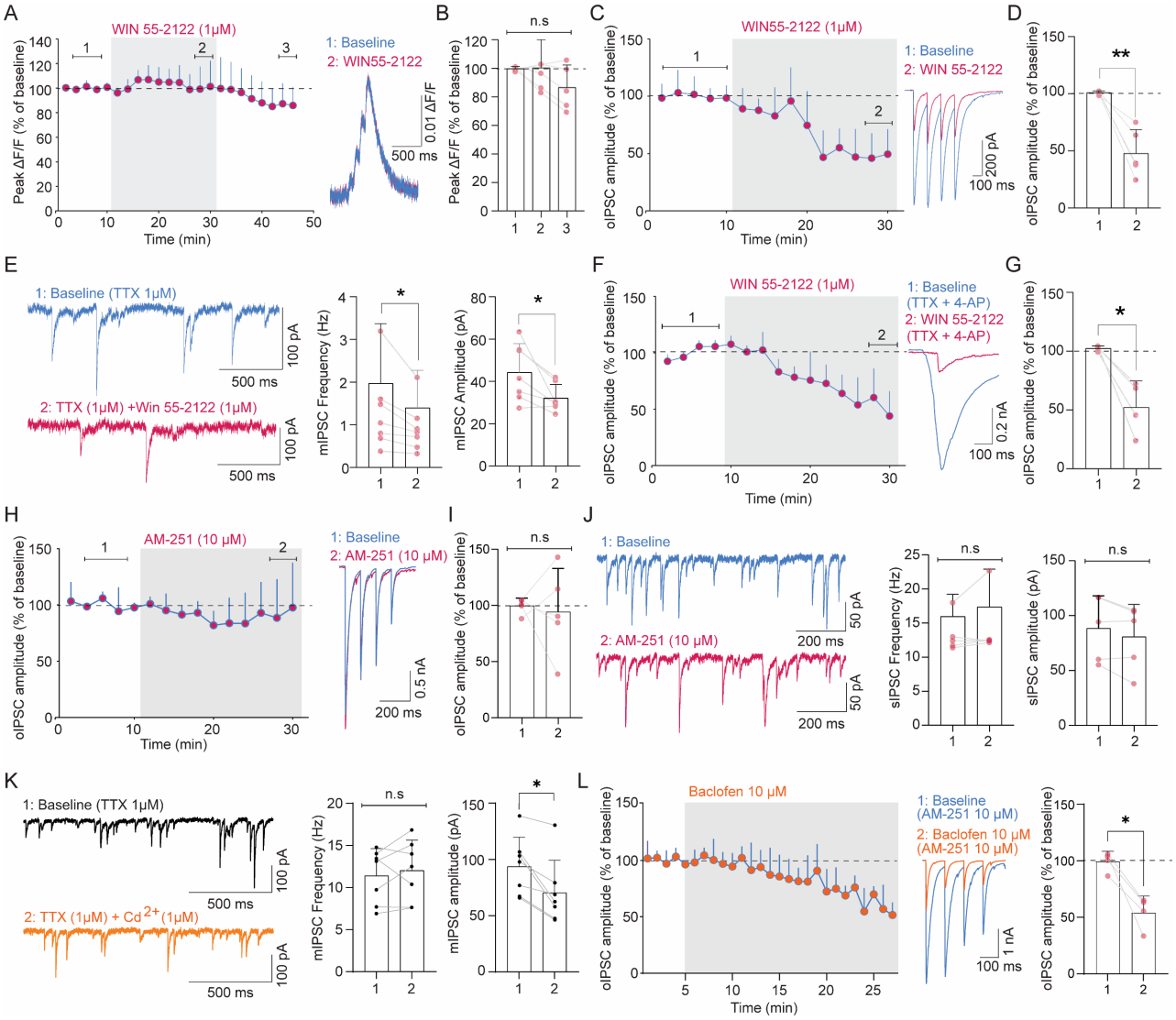

Figure 4: VGCC- and KV1-independent mechanisms of presynaptic modulation of iSPN-GPe projections by CB1 receptors. Time course of WIN effects on PreCaTs and raw photometry traces. **B:** Summary of drug effects: baseline, last 2 minutes of drug, last 2 minutes of washout. CB1 receptor activation (WIN 55-2122, n = 5 slices from n = 4 mice) did not change PreCaTs amplitude. **C:** Time course of WIN effects on oIPSCs at iSPN-GPe synapses and raw electrophysiological traces). **D:** WIN 55-2122 application significantly decreased oIPSC amplitude (n = 5 cells from n = 5 mice). **E:** Effects of WIN 55-2122 application on mIPSCs. Example traces and summary bar graphs. WIN 55-2122 application significantly decreased the frequency and amplitude of mIPSCs (n= 7 cells from n = 4 mice) **F**: Time course of WIN 55-2122 effects on oIPSCs recorded in the presence of TTX + 4AP. **G**: WIN 55-2122 significantly reduced oIPSCs at iSPN-GPe terminals (n = 4 cells from n = 3 mice). **H, I:** No effect of AM-251 application on oIPSCs (n = 5 cells from n = 3 mice). **J**: No effect of AM-251 application on sIPSC frequency or amplitude (n= 5 cells from n = 3 mice). **K**: Cd^{2+} decreased the amplitude but not frequency of mIPSCs (n = 7 cells from n = 3 mice). **L**: Baclofen effects were preserved in slices pre-incubated with AM-251 (n = 4 cells from n = 2 mice). * $p < 0.05$; ** $P < 0.011$.

374 We next studied the effects of CB1 receptor activation on PreCaTs at iSPN-GPe projections (Fig. 4 A, B). Bath
375 application of the CB1 agonist WIN 55212-2 did not change PreCaTs amplitude, which was 100.3 + 19.7 % of
376 baseline following WIN 55212-2 application and 86.6 + 15.7 % of baseline after washout (n = 5 slices from n = 4
377 mice, one-way rmANOVA, Treatment: $F_{(2, 8)} = 2.386$; $p = 0.154$). We next asked whether CB1 receptors reduced
378 GABAergic transmission specifically at iSPN-GPe synapses (Fig. 4C, D). Bath application of WIN 55212-2
379 decreased the oIPSC amplitude to 47.8 + 20.8 % of baseline (n = 5 cells from n = 5 mice, paired t-test, p = 0.0053).
380 CB1 activation did not decrease PreCaTs while inhibiting GABAergic transmission at iSPN-GPe projections. Next,
381 we recorded mIPSCs in presence of the Na_V blocker TTX (Fig. 4E). Bath application of WIN 55212-2 decreased
382 the mIPSC frequency from 2 + 1.4 Hz to 1.4 + 0.88 Hz (n = 7 cells from n = 4 mice, paired t-test, p = 0.0314) and
383 decreased the mIPSC amplitude from 44.3 + 13.6 pA to 31.1 + 6.5 pA (n = 7 cells from n = 4 mice, paired t-test, p
384 = 0.025). This indicates a presynaptic effect of CB1 receptor activation on GABA release in the GPe, but a change
385 in amplitude might be indicative of an additional postsynaptic contribution, an effect on multivesicular release or a
386 shift in the population of synapses contributing to the mIPSCs. We tested whether CB1 receptor effects at iSPN-
387 GPe synapses might be mediated by K_V1 channels, as suggested for glutamatergic synapses in the nucleus
388 accumbens (Robbe et al., 2001) and cerebellar parallel fibers (Daniel et al., 2004). We examined WIN 55-2122
389 effects by recording baseline and drug application in aCSF containing the K_V1 channel blocker 4-AP and TTX.
390 Under these experimental conditions hChR2-evoked presynaptic depolarization is independent of Na_V channels and
391 K_V channels, and monosynaptic connectivity is isolated (Cho et al., 2013; Petreanu et al., 2009). We found that WIN
392 55212-2 application produced a reduction of oIPSC amplitude to 52.3 + 22. 5 % of baseline (n = 4 cells from n = 3
393 mice, paired t-test, p = 0.0216) (Fig. 4F; G). These experiments indicate that CB1 effects on iSPN-GPe projections
394 are monosynaptic and not mediated through the inhibition of K_V1 or Na_V channels. To test whether an
395 endocannabinoid tone is present on iSPN-GPe projections, we bath applied the CB1 antagonist AM-251. We found
396 that AM-251 (10 μM) application did not significantly change the amplitude of oIPSCs (amplitude: 94.3 + 38.6 %
397 of baseline after AM-251; paired t-test, p = 0.776), nor the amplitude and frequency of sIPSCs recorded in the GPe
398 (Fig 4H-I-J) (n = 5 cells from n = 3 mice; frequency: baseline 16 + 3.2 Hz, AM-251 17.4 + 5.5 Hz; paired t-test, p
399 = 0.2767; amplitude: baseline 88.5 + 29.6 pA, AM-251 80.7 + 29.6 pA; paired t-test, p = 0.1159).
400 To test for a possible contribution of VGCCs to mIPSCs in the GPe, we studied the effects of the non-specific
401 VGCC blocker Cd^{2+} on mIPSCs (Fig. 4K). We found that Cd^{2+} application did not change the frequency of mIPSCs
402 in the GPe (n = 7 cells from n = 3 mice; baseline: 11.4 + 3.2 Hz; Cd^{2+}: 12 + 3.6 Hz; paired t-test, p = 0.4728), ruling
403 out presynaptic effects of Cd^{2+}. Cd^{2+} application decreased the amplitude of mIPSCs in the GPe (n = 7 cells from n
404 = 3 mice; baseline 93.7 + 26 pA; Cd^{2+} 70.3 + 28.9 pA; Wilcoxon signed-rank test, p = 0.0156), indicating a possible
405 post-synaptic effect of Cd^{2+} mediated by direct Cd^{2+} modulation of $GABA_A$ receptors (Molnár et al., 2004) or
406 indirect by altered Ca^{2+}- dependent modulation of $GABA_A$ receptors (Grayelle et al., 2021). Taken together, Na_V
407 independent GABA release in the GPe is independent from VGCCs.

408 Finally, we sought to establish if a cross- talk exist between $GABA_B$ and CB1 receptors on iSPN-GPe projections.
409 In a subset of cells from the experiments in Fig. 4H, AM-251 bath application was followed by the bath application
410 of Baclofen. We found that bath application of Baclofen (10 μM) in presence of AM-251 (10 μM) significantly
411 decreased the oIPSC amplitude to 54.19 + 14.6 % of baseline (Fig. 4L) (n = 4 cells from n = 2 mice; paired t-test,
412 p = 0.0149). Taken together, these results indicate that CB1 receptors control iSPN-GPe projections through a
413 mechanism independent from VGCCs, K_V1 or Na_V channels. Furthermore, we found no evidence for cross-talk
414 between $GABA_B$ and CB1 receptor mediated control of GABA release on iSPN-GPe projections.
415

416 **Discussion**

417 Here we used a combination of brain slice photometry and whole-cell patch clamp to study the presynaptic
418 modulation of indirect pathway projections (iSPN-GPe) by CB1 and $GABA_B$ receptors. We first determined that
419 Presynaptic Calcium Transients (PreCaTs) and GABA release at striatal iSPN-GPe terminals are primarily mediated
420 by P/Q-type VGCCs. $GABA_B$ receptors modulate PreCaTs and GABA release at these terminals through a
421 presynaptic mechanism. CB1 receptors control GABA release but not PreCaTs through a VGCC-, Na_V and K_V1
422 independent presynaptic mechanism. We found no evidence of cross- talk between $GABA_B$ and CB1 receptors on
423 iSPN-GPe projections. Our results indicate that $GABA_B$ and CB1 receptors mediate presynaptic inhibition at iSPN-
424 GPe synapses through distinct mechanisms.

425 We focused our experiments on the study of presynaptic modulation of iSPN-GPe projections assuming similar
426 principles governing PreCaTs and GABA release at iSPN-GPe synapses on distinct GPe neuronal populations.
427 However, presynaptic modulation of iSPN projections might be recruited with specific modalities by different
428 neuronal populations of GPe neurons.

429 <u>Control of presynaptic Ca^{2+} at iSPN-GPe projections</u>

430 We studied PreCaTs at iSPN-GPe projections using a genetic approach to express GCaMP6f in iSPNs. As a result,
431 GCaMP6f was expressed in iSPNs independently from their location in striatal subregions (dorsomedial,
432 ventromedial, or dorsolateral striatum) or the molecularly defined striatal subcompartments, patch and matrix.
433 Using field photometry and pharmacology we were able to measure activity- dependent PreCaTs and determine
434 which VGCCs subtypes mediate them. Further, we could study their modulation by $GABA_B$ and CB1 receptors.
435 Field photometry allowed the measurement of PreCaTs in a selected field of view within the GPe containing iSPN
436 axons. This population-level measurement likely reflects the sum of axonal Ca^{2+} proximal to, and distal from,
437 presynaptic terminals/ release sites given the widespread expression of the fluorescent indicator throughout the
438 axon. A limitation of this approach is that the spatial resolution of field photometry might not be sufficient to reflect
439 small Ca^{2+} variations restricted to the presynaptic terminals but critical for neurotransmitter release. To counter this
440 limitation, we generated mice genetically expressing hChR2 in iSPNs and performed patch-clamp recordings to

441 measure neurotransmitter release. This approach ensured high temporal and spatial resolution allowing us to
442 examine monosynaptic iSPN-GPe projections.

443 The use of whole cell patch-clamp allowed us to study activity- dependent neurotransmitter release and its control
444 by VGCCs, $GABA_B$ and CB1 receptors. It also allowed to measure action potential-independent, VGCC-
445 independent neurotransmitter release by recording mIPSCs in the presence of the Na_V blocker TTX. We found that
446 mIPSC frequency was insensitive to the blockade of VGCCs by Cd^{2+} indicating that mIPSCs in the GPe are VGCC-
447 independent. Taken together, a combination of field photometry, whole cell patch-clamp and optogenetics allowed
448 us to gain mechanistic insights on the modulation of iSPN projections by GPCRs. In the present study we examined
449 GPCR modulation using bath application of agonists. While this approach ensures uniform concentrations of agonist
450 throughout the preparation, the drug application time and washout are much slower than with other techniques (e.g.
451 rapid, local agonist application). In addition, while there is the possibility with this approach that agonist actions
452 may occur at sites other than the presynaptic terminal of the synapse under study, this concern is mitigated to some
453 extent by the examination of sIPSCs in the presence of TTX which will reduce many neuronal interactions that
454 could give rise to indirect effects, as well as the pharmacological isolation of ISPCs that reduces influences from
455 glutamatergic synapses.

456 We found that PreCaTs were inhibited by an antagonist of P/Q type VGCC, but not by antagonists of N-type or L-
457 type VGCC. GABA release was decreased by antagonists of P/Q type and to a smaller extent by antagonists of N-
458 type or L-type VGCCs. One possibility is that small variations in presynaptic Ca^{2+} that were not detectable using
459 slice photometry contributed to the effects of N-type of L-type antagonists on GABA release.

460 <u>Control of iSPN-GPe projections by $GABA_B$ receptors</u>

461 We found that $GABA_B$ receptors modulate the iSPN-GPe projection by suppressing GABA release and PreCaTs.
462 $GABA_B$ receptor activation decreased sIPSC frequency in the GPe, indicating a presynaptic site of action. A
463 decrease in sIPSC frequency and amplitude does not exclude $GABA_B$ receptor-mediated inhibition of other
464 GABAergic inputs to the GPe, including local collaterals, bridge collateral dSPN projections and GPi inputs. A
465 decrease in sIPSC amplitude might result from the inhibition of selected GABAergic inputs or from the reduction
466 of multi-vesicular release. Alternatively, these changes may emerge from post-synaptic $GABA_B$ mediated effects
467 (Kaneda & Kita, 2005). Our results are consistent with previous reports indicating VGCCs as one of the downstream
468 targets of $GABA_B$ receptor signaling at corticostriatal synapses (Kupfershmidt & Lovinger, 2015) granule-Purkinje
469 cell cerebellar synapses (Dittman & Regehr, 1996) and hippocampal synapses (Doze et al., 1995; Wu & Saggau,
470 1995). Ultrastructural studies have identified the expression of $GABA_B$ receptors in the GPe in rodents and primates.
471 Pre-synaptic $GABA_B$ receptors were found on GABAergic inputs to the GPe and on anterogradely labelled
472 striatopallidal projections (Charara et al., 1999; Chen et al., 2004). Further, $GABA_B$ receptors were found post-
473 synaptically at GABAergic synapses and presynaptically at glutamatergic synapses in the GPe (Chen et al., 2004).

474 Hence, $GABA_B$ receptors are positioned to regulate GPe physiology as autoreceptors, heteroreceptors or
475 postsynaptic receptors. In our recording conditions, no $GABA_B$ mediated postsynaptic responses were observed
476 since GIRK channels were blocked by including Cs^+ in the intracellular recording solution.
477
478 Control of iSPN-GPe projections by CB1 receptors
479 Our results indicate that CB1 receptors modulate iSPN-GPe projections by reducing GABA release while our slice
480 photometry experiments indicated no effect of CB1 receptor activation on presynaptic Ca^{2+}. Further, we found that
481 bath application of the CB1 agonist WIN 55212-2 induced a decreased mIPSC frequency and reduced the amplitude
482 of oIPSCs recorded in presence of K_V1 and Na_V antagonists. Overall, our presynaptic Ca^{2+} measurements and
483 neurotransmitter release measurements converged in indicating a VGCC-independent, Na_V and K_V1 independent
484 control of GABA release by CB1 receptors on iSPN projections to the GPe. These results reproduce, extend, and
485 provide synapse specificity to previously published work on the inhibitory effect of CB1 receptors on GABAergic
486 synaptic transmission in the GPe (Engler et al., 2006). Engler and colleagues reported a CB1-mediated inhibition
487 of presynaptic calcium at striatopallidal synapses, while we observed no CB1- mediated inhibition of PreCaTs.
488 These discrepant results might be due to differences in the slice preparation used, differences between mouse strains,
489 and differences in analysis methods used to determine PreCaTs. We found no evidence for a CB1- mediated tonic
490 inhibition of GABA release on iSPN-GPe projections indicating that the lack of effect of the CB1 agonist WIN
491 55212-2 in our experiments is not 'masked' by a tone. CB1 receptors have been proposed to suppress
492 neurotransmitter release through the activation of K_V channels at cortico-accumbal (Robbe et al., 2001) and
493 cerebellar parallel fiber synapses (Daniel et al., 2004). CB1-mediated inhibition of Na_V- independent GABA release
494 in the DS was also observed (Adermark et al., 2009). Other studies proposed that presynaptic CB1 receptors depress
495 glutamate release at corticostriatal through the inhibition of N-type Ca^{2+} channels (Huang et al., 2001), and a similar
496 VGCC-dependent action was reported at hippocampal GABAergic synapses (Hoffman & Lupica, 2001). CB1
497 receptors were also shown to depress presynaptic Ca^{2+} influx at cerebellar granule-Purkinje cell synapses (Brown
498 et al., 2004), as well as Ca^{2+} currents at calyx of Held synapses in the auditory brainstem (Kushmerick et al., 2004).
499 The signaling cascade recruited by CB1 receptor activation on iSPN-GPe terminals remains to be fully elucidated.
500 A possible alternative mechanism might involve the direct interaction of the $G_{B\gamma}$ subunit with SNARE complexes.
501 It has been proposed that $G_{B\gamma}$ subunits can target the C-terminus domain of SNAP-25 (Zurawski et al., 2019). This
502 mechanism has been shown to mediate effects of the 5HT1B receptor in the hippocampus, and the α2a adrenergic
503 receptor on glutamatergic synapses in the BNST, (Zurawski et al., 2019), as well as effects of $GABA_B$ receptors on
504 glutamatergic inputs to SPNs in the nucleus accumbens (Manz et al., 2019). However, CB1 receptors have not yet
505 been shown to activate this signaling cascade. A different possibility comes from a study that examined CB1-
506 mediated control of GABA release at dSPN-SNr projections (Soria-Gomez et al., 2021). The authors found that
507 CB1 receptors reside on the plasma membrane and on mitochondria in this projection. Plasma membrane-associated

508 CB1 receptors controlled substance P release via inhibition of cytosolic PKA, whereas mitochondria associated
509 CB1 receptors controlled GABA release via inhibition of mitochondrial PKA.
510 Here, we found that CB1 signaling at iSPN-GPe synapses is non- VGCC dependent, fitting with a growing
511 complexity of CB1 receptor mediated signaling in the CNS.

512 What is the functional significance of CB1 receptor signaling on iSPN-GPe terminals? The levels of the CB1
513 receptor in the GPe are among the highest in the CNS. CB1 receptors expressed in SPNs control locomotor and
514 exploratory behavior (Bonm et al., 2021). The endocannabinoids anandamide and 2-arachidonoylglycerol (2-AG)
515 were detected in the rat GPe (Di Marzo et al., 2000) but the mechanisms driving their release remains unclear. Local
516 microinjections of synthetic cannabinoids in the GPe were found to increase ipsilateral rotations (Sañudo-Peña et
517 al., 1999) and to enhance muscimol-induced catalepsy (Pertwee & Wickens, 1991). Further, reserpine treatment
518 enhanced anandamide and 2-AG levels in the rat GPe (Di Marzo et al., 2000). CB1 receptors in the GPe might be
519 primarily recruited by endocannabinoids released retrogradely. Alternatively, astrocytes surrounding striatopallidal
520 projections (Galvan et al., 2010) might provide an alternative source of endocannabinoids, although these remain
521 untested hypotheses. A third possibility involves endocannabinoid production and release at iSPN-GPe synapses
522 recruited by neuromodulatory or glutamatergic inputs to the GPe. We did not find any evidence of endocannabinoid
523 activation of CB1 receptors on striatopallidal neurons under the afferent stimulation or sIPSC recording conditions
524 in this study. However, other patterns of afferent and neuronal activation need to be explored, perhaps with the help
525 of newly developed endocannabinoid sensors (Dong et al., 2022).
526

527 We show that CB1 and $GABA_B$ receptors recruit distinct presynaptic signaling mechanisms. By inhibiting VGCCs,
528 $GABA_B$ receptors might shunt action potential evoked neurotransmitter release at iSPN-GPe synapses, in response
529 to increased presynaptic activity (autoreceptor role) or increased local GABA (heteroreceptor role). CB1 receptors
530 might function synergistically with $GABA_B$ receptors by further decreasing GABA release from striatopallidal
531 synapses. We found that pre-incubation of the slices with a CB1 receptor antagonist did not prevent the effects of
532 the $GABA_B$ agonist, baclofen, indicating no cross talk between $GABA_B$ and CB1 receptors at iSPN-GPe projections.
533 The growing understanding of the GPe cell-type composition, connectivity, microcircuitry and function requires a
534 synapse-specific approach to contextualize the role of CB1 and $GABA_B$ receptor signaling in this region. A detailed
535 analysis of the striato-pallidal and pallido-pallidal circuitry has proposed that iSPN-GPe projections are the densest
536 in the GPe and primarily target prototypic over arkypallidal GPe neurons (Cui et al., 2021; Ketzef & Silberberg,
537 2021). PV+ neurons represent the primary source of collateral inhibition in the GPe (Cui et al., 2021; Higgs et al.,
538 2021; Ketzef & Silberberg, 2021). Presynaptic inhibition of iSPN-GPe projections might therefore produce
539 primarily a disinhibition of the output of GPe prototypic neurons to the SNr, Subthalamic Nucleus and
540 Parafascicular Thalamus (Lilasharoen et al., 2020; Pamukcu et al., 2020) in addition to disinhibiting local

collaterals. Presynaptic modulation will ultimately contribute to determine the GPe behavioral output, contributing to movement control and action selection.

Conclusion

In conclusion, our results indicate that distinct mechanisms of presynaptic modulation are recruited by CB1 and $GABA_B$ receptors on the striatal indirect pathway projections to the GPe. Presynaptic modulation by CB1 and $GABA_B$ receptors decrease the synaptic efficacy of iSPN-GPe projections by inhibiting GABA release and ultimately contributes to shape the basal ganglia output. Our results encourage research on the synapse-specific mechanisms of Gi/o coupled receptor signaling which might inform the development of targeted pharmacological treatments for movement and psychiatric disorders.

Author contributions

KPA, DL, GS and DML were responsible for the conception and design of the study. KPA, DL, GS performed electrophysiological recordings. GS analyzed electrophysiological recordings. KPA, DL and GMC performed slice photometry experiments and analyses. GS performed and analyzed immunohistochemical experiments. GS drafted the manuscript and the figures with inputs from all authors and all authors gave final approval.

Acknowledgments

This work was supported by the National Institutes of Health, National Institute on Alcohol Abuse and Alcoholism, Division of Intramural Clinical and Biological Research (ZIAAA000416). We thank the NIAAA animal care stuff for their precious support for animal husbandry and veterinary care. We thank Guoxiang Luo for genotyping assistance, and all the Laboratory for Integrative Neurosciences for the helpful discussions.

Data availability statement

All data generated or analyzed in this manuscript are included in the manuscript and its supplementary file(s).

575 **References**

576 Adermark L, Talani G & Lovinger DM (2009). Endocannabinoid-dependent plasticity at GABAergic
577 and glutamatergic synapses in the striatum is regulated by synaptic activity. *European Journal of*
578 *Neuroscience* **29,** 32–41.

579 Araque A, Castillo PE, Manzoni OJ & Tonini R (2017). Synaptic functions of endocannabinoid
580 signaling in health and disease. *Neuropharmacology* **124,** 13–24.

581 Bonm AV, Elezgarai I, Gremel CM, Viray K, Bamford NS, Palmiter RD, Grandes P, Lovinger DM &
582 Stella N (2021). Control of exploration, motor coordination and amphetamine sensitization by
583 cannabinoid CB_1 receptors expressed in medium spiny neurons. *Eur J of Neuroscience* **54,**
584 4934–4952.

585 Brown SP (2004). Endocannabinoids Inhibit Transmission at Granule Cell to Purkinje Cell Synapses by
586 Modulating Three Types of Presynaptic Calcium Channels. *Journal of Neuroscience* **24,** 5623–
587 5631.

588 Chalifoux JR & Carter AG (2011). GABAB receptor modulation of synaptic function. *Current Opinion*
589 *in Neurobiology* **21,** 339–344.

590 Chang HT, Wilson CJ & Kitai ST (1981). Single neostriatal efferent axons in the globus pallidus: a light
591 and electron microscopic study. *Science* **213,** 915–918.

592 Charara A, Heilman C, Levey AI & Smith Y (1999). Pre- and postsynaptic localization of GABAB
593 receptors in the basal ganglia in monkeys. *Neuroscience* **95,** 127–140.

594 Chen L, Boyes J, Yung W-H & Bolam JP (2004). Subcellular localization of GABAB receptor subunits
595 in rat globus pallidus. *J Comp Neurol* **474,** 340–352.

596 Cho J-H, Deisseroth K & Bolshakov VY (2013). Synaptic Encoding of Fear Extinction in mPFC-
597 amygdala Circuits. *Neuron* **80,** 1491–1507.

598 Cui Q, Du X, Chang IYM, Pamukcu A, Lilascharoen V, Berceau BL, García D, Hong D, Chon U,
599 Narayanan A, Kim Y, Lim BK & Chan CS (2021). Striatal Direct Pathway Targets $Npas1^{+}$
600 Pallidal Neurons. *J Neurosci* **41,** 3966–3987.

601 Daniel H, Rancillac A & Crepel F (2004). Mechanisms underlying cannabinoid inhibition of presynaptic
602 Ca^{2+} influx at parallel fibre synapses of the rat cerebellum: CB1-mediated control of presynaptic
603 Ca^{2+} influx. *The Journal of Physiology* **557,** 159–174.

604 Davis MI, Crittenden JR, Feng AY, Kupferschmidt DA, Naydenov A, Stella N, Graybiel AM &
605 Lovinger DM (2018). The cannabinoid-1 receptor is abundantly expressed in striatal striosomes
606 and striosome-dendron bouquets of the substantia nigra. *PLoS One* **13,** e0191436.

607 Di Marzo V (2000). Enhanced levels of endogenous cannabinoids in the globus pallidus are associated
608 with a reduction in movement in an animal model of Parkinson's disease. *The FASEB Journal*
609 **14,** 1432–1438.

610 Dittman J & Regehr W (1996). Contributions of calcium-dependent and calcium-independent
611 mechanisms to presynaptic inhibition at a cerebellar synapse. *J Neurosci* **16,** 1623–1633.

612 Dong A, He K, Dudok B, Farrell JS, Guan W, Liput DJ, Puhl HL, Cai R, Wang H, Duan J, Albarran E,
613 Ding J, Lovinger DM, Li B, Soltesz I & Li Y (2022). A fluorescent sensor for spatiotemporally
614 resolved imaging of endocannabinoid dynamics in vivo. *Nat Biotechnol* **40,** 787–798.

615 Doze VA, Cohen GA & Madison DV (1995). Calcium channel involvement in GABAB receptor-
616 mediated inhibition of GABA release in area CA1 of the rat hippocampus. *Journal of*
617 *Neurophysiology* **74,** 43–53.

618 Engler B, Freiman I, Urbanski M & Szabo B (2006). Effects of Exogenous and Endogenous
619 Cannabinoids on GABAergic Neurotransmission between the Caudate-Putamen and the Globus
620 Pallidus in the Mouse. *J Pharmacol Exp Ther* **316,** 608–617.

621 Galvan A, Hu X, Smith Y & Wichmann T (2010). Localization and function of GABA transporters in
622 the globus pallidus of parkinsonian monkeys. *Experimental Neurology* **223,** 505–515.

623 Gerfen CR, Engber TM, Mahan LC, Susel Z, Chase TN, Monsma FJ & Sibley DR (1990). D1 and D2
624 dopamine receptor-regulated gene expression of striatonigral and striatopallidal neurons. *Science*
625 **250,** 1429–1432.

626 Graveland GA & Difiglia M (1985). The frequency and distribution of medium-sized neurons with
627 indented nuclei in the primate and rodent neostriatum. *Brain Research* **327,** 307–311.

628 Gravielle MC (2021). Regulation of GABAA Receptors Induced by the Activation of L-Type Voltage-
629 Gated Calcium Channels. *Membranes* **11,** 486.

630 Herkenham M, Lynn AB, de Costa BR & Richfield EK (1991). Neuronal localization of cannabinoid
631 receptors in the basal ganglia of the rat. *Brain Research* **547,** 267–274.

632 Higgs MH, Jones JA, Chan CS & Wilson CJ (2021). Periodic unitary synaptic currents in the mouse
633 globus pallidus during spontaneous firing in slices. *J Neurophysiol* **125,** 1482–1500.

634 Hoffman AF & Lupica CR (2000). Mechanisms of Cannabinoid Inhibition of $GABA_A$ Synaptic
635 Transmission in the Hippocampus. *J Neurosci* **20,** 2470–2479.

636 Hu SS-J & Mackie K (2015). Distribution of the Endocannabinoid System in the Central Nervous
637 System. In *Endocannabinoids*, ed. Pertwee RG, Handbook of Experimental Pharmacology, pp.
638 59–93. Springer International Publishing, Cham.

639 Huang C, Lo S & Hsu K (2001). Presynaptic mechanisms underlying cannabinoid inhibition of
640 excitatory synaptic transmission in rat striatal neurons. *The Journal of Physiology* **532,** 731–748.

641 Kaneda K & Kita H (2005). Synaptically Released GABA Activates Both Pre- and Postsynaptic GABA
642 B Receptors in the Rat Globus Pallidus. *Journal of Neurophysiology* **94,** 1104–1114.

643 Ketzef M & Silberberg G (2021). Differential Synaptic Input to External Globus Pallidus Neuronal

644 Subpopulations In Vivo. *Neuron* **109,** 516-529.e4.

645 Kupferschmidt DA & Lovinger DM (2015). Inhibition of presynaptic calcium transients in cortical
646 inputs to the dorsolateral striatum by metabotropic GABA $_B$ and mGlu2/3 receptors. *J Physiol*
647 **593,** 2295–2310.

648 Kushmerick C (2004). Retroinhibition of Presynaptic Ca2+ Currents by Endocannabinoids Released via
649 Postsynaptic mGluR Activation at a Calyx Synapse. *Journal of Neuroscience* **24,** 5955–5965.

650 Lilascharoen V, Wang EH-J, Do N, Pate SC, Tran AN, Yoon CD, Choi J-H, Wang X-Y, Pribiag H, Park
651 Y-G, Chung K & Lim BK (2021). Divergent pallidal pathways underlying distinct Parkinsonian
652 behavioral deficits. *Nat Neurosci* **24,** 504–515.

653 Manz KM, Baxley AG, Zurawski Z, Hamm HE & Grueter BA (2019). Heterosynaptic GABA $_B$
654 Receptor Function within Feedforward Microcircuits Gates Glutamatergic Transmission in the
655 Nucleus Accumbens Core. *J Neurosci* **39,** 9277–9293.

656 Molnár G, Salánki J & Kiss T (2004). Cadmium inhibits GABA-activated ion currents by increasing
657 intracellular calcium level in snail neurons. *Brain Research* **1008,** 205–211.

658 Pamukcu A, Cui Q, Xenias HS, Berceau BL, Augustine EC, Fan I, Chalasani S, Hantman AW, Lerner
659 TN, Boca SM & Chan CS (2020). Parvalbumin+ and Npas1+ Pallidal Neurons Have Distinct
660 Circuit Topology and Function. *J Neurosci* **40,** 7855–7876.

661 Pertwee RG & Wickens AP (1991). Enhancement by chlordiazepoxide of catalepsy induced in rats by
662 intravenous or intrapallidal injections of enantiomeric cannabinoids. *Neuropharmacology* **30,**
663 237–244.

664 Petreanu L, Mao T, Sternson SM & Svoboda K (2009). The subcellular organization of neocortical
665 excitatory connections. *Nature* **457,** 1142–1145.

666 Robbe D, Alonso G, Duchamp F, Bockaert J & Manzoni OJ (2001). Localization and Mechanisms of
667 Action of Cannabinoid Receptors at the Glutamatergic Synapses of the Mouse Nucleus
668 Accumbens. *J Neurosci* **21,** 109–116.

669 Sañudo-Peña MC, Tsou K & Walker JM (1999). Motor actions of cannabinoids in the basal ganglia
670 output nuclei. *Life Sciences* **65,** 703–713.

671 Soria-Gomez E et al. (2021). Subcellular specificity of cannabinoid effects in striatonigral circuits.
672 *Neuron* **109,** 1513-1526.e11.

673 Weglage M, Ährlund-Richter S, Fuzik J, Skara V, Lazaridis I & Meletis K (2022). *Sst+ GPi output*
674 *neurons provide direct feedback to key nodes of the basal ganglia and drive behavioral*
675 *flexibility*. Neuroscience. Available at: http://biorxiv.org/lookup/doi/10.1101/2022.03.16.484460

676 Wu LG & Saggau P (1995). GABAB receptor-mediated presynaptic inhibition in guinea-pig
677 hippocampus is caused by reduction of presynaptic Ca2+ influx. *The Journal of Physiology* **485,**
678 649–657.

679 Zurawski Z, Thompson Gray AD, Brady LJ, Page B, Church E, Harris NA, Dohn MR, Yim YY, Hyde
680 K, Mortlock DP, Jones CK, Winder DG, Alford S & Hamm HE (2019). Disabling the Gβγ-
681 SNARE interaction disrupts GPCR-mediated presynaptic inhibition, leading to physiological and
682 behavioral phenotypes. *Sci Signal* **12,** eaat8595.

683